Single crystal Raman spectroscopy of natural leiteite $ZnAs_2O_4$ and in comparison with the synthesised mineral

Silmarilly Bahfenne, Llew Rintoul and Ray L. Frost •

Chemistry, Faculty of Science and Technology, Queensland University of Technology, GPO Box 2434, Brisbane Queensland 4001, Australia.

ABSTRACT

The oriented single crystal Raman spectrum of leiteite has been obtained and the spectra related to the structure of the mineral. The intensities of the observed bands vary according to orientation allowing them to be assigned to either A_g or B_g modes. A_g bands are generally the most intense in the CAAC spectrum, followed by ACCA, CBBC, and ABBA whereas B_g bands are generally the most intense in the CBAC followed by ABCA. The CAAC and ACCA spectra are identical, as are those obtained in the CBBC and ABBA orientations. Both cross-polarised spectra are identical. Band assignments were made with respect to bridging and non-bridging As-O bonds.

KEYWORDS: arsenite, leiteite, reinerite, Raman Spectroscopy, single crystal

• Author to whom correspondence should be addressed (r.frost@qut.edu.au)

INTRODUCTION

The zinc arsenite mineral leiteite has the formula $ZnAs_2O_4$ and is monoclinic with space group $P2_1/c$ and Z = 4 (a = 4.542, b = 5.022, c = 17.597 Å) and β =90.81° [1]. It occurs as brown to colourless transparent flakes with a pearlescent appearance. Leiteite is a zinc meta arsenite, which has been prepared in a laboratory as wood preservative and insecticide. Meta arsenite compounds that have been previously studied include $NaAsO_2$ [2, 3] and $CuAs_2O_4$ or trippkeite [4-7]. In the above compounds the arsenite group is not isolated, rather polymerised via their vertices. The structure of claudetite, the monoclinic modification of As_2O_3, is also comparable to those of meta arsenites; it consists of an infinite zigzag chain of alternating As and O. Although trippkeite $CuAs_2O_4$ [8, 9] and the isostructural schafarzikite $Fe^{2+}Sb_2O^4$ [10-13] both have infinite arsenite or antimonite chains, leiteite is the only known mineral of its kind. In the first two the cation is found in an octahedral geometry whereas Zn is in a tetrahedral geometry in leiteite. Furthermore the bridging O atoms in the arsenite group of leiteite bind only to As atoms; one bridging O in trippkeite and schafarzikite is connected to a Cu or Fe atom as well as two As or Sb atoms.

A review of the vibrational spectroscopy of arsenite and antimonite minerals has been undertaken [14] Some recent studies of arsenite minerals have been published by the authors. [15-18] Although Raman studies on aqueous solutions of arsenic trioxide have spanned several decades, few spectroscopic investigations have been undertaken on other arsenite minerals and none to date on leiteite [18]. Certainly no single crystal studies of these types of minerals has ever been undertaken.

EXPERIMENTAL

Minerals

Crystals of leiteite were supplied by The Mineralogical Research Company and Museum Victoria. The mineral originated from the Tsumeb mine, Tsumeb, Otavi District, Oshikoto, Namibia

Synthesis of leiteite

Synthetic leiteite was prepared following the procedures given by Curtin. 16.7429 g (0.0583 mol) of $ZnSO_4.7H_2O$ was dissolved in 100 mL deionised H_2O, followed by two drops glacial

CH_3COOH. Another solution is made up consisting of 200 mL deionised H_2O and 12.5981 g (0.0639 mol) As_2O_3. To assist dissolution of As_2O_3 in H_2O 0.5800 g of Na_2CO_3 was added and heat was applied to boil the solution. After dissolution the temperature was allowed to decrease to below 50°C after which 5.294 g (0.0555 mol in total) of Na_2CO_3 was added. The latter solution ($NaAsO_2$) is added to the former with good agitation. Snow white crystals of $ZnAs_2O_4$ precipitated immediately, separated by filtration, washed with deionised water, and dried at 150°C overnight. Note that the glacial CH_3COOH was added to prevent the initial precipitation of zinc ortho arsenite also known as the mineral reinerite or $Zn_3(AsO_3)_2$. When CH_3COOH was not present, leiteite was still the major component of the reaction but reinerite was also present as an impurity.

X-ray diffraction

The crystalline materials were characterised by X-ray powder diffraction (XRD). The XRD analyses were carried out on a Philips wide-angle PW 1050/25 vertical goniometer (Bragg Brentano geometry) applying CuKα radiation (λ = 1.54 Å, 40 kV, 40 mA). The samples were measured in step scan mode with steps of 0.02° 2θ and a scan speed of 1.00° per minute from 2 to 75° 2θ.

Scanning electron microscopy

Scanning electron microscope (SEM) photos were obtained on a FEI QUANTA 200 Environmental Scanning Electron Microscope operating at high vacuum and 15 kV. This system is equipped with an Energy Dispersive X-ray spectrometer with a thin Be window capable of analysing all elements of the periodic table down to carbon. For the analysis a counting time of 100 s was applied. A small clear flake of natural leiteite was coated in gold and the SEM images show the platy nature of the mineral, the flat surface being the (001) plane

Raman microscopy

The instrument used was a Renishaw 1000 Raman microscope system,
which also includes a monochromator, a Rayleigh filter system and a CCD detector coupled to an Olympus BHSM microscope equipped with 10x, and 50x
objectives. The Raman spectra were excited by a Spectra-Physics model 127 He-Ne laser producing plane polarised light at 633 nm and collected at a resolution of better than 4 cm^{-1} and a precision of ± 1 cm^{-1} in the range between 120 and 4000 cm^{-1}. Repeated acquisitions on

the crystals using the highest magnification (50x) were accumulated to improve the signal-to-noise ratio in the spectra. The instrument was calibrated prior to use using the 520.5 cm^{-1} line of a silicon wafer.

A crystal of leiteite was selected and placed on the corner of a perfect cube, aligned parallel to the sides of the cube using a very fine needle. The rotation of the cube through 90° about the X, Y, Z axes of the laboratory frame allowed the determination of the three crystallographic axes. The crystal flake lay flat on its perfect (001) cleavage plane with the *c* axis almost perpendicular to the plane. Since $\beta = 90.82°$ this slight misalignment between the c axis and the laboratory frame was ignored. In the plane of the leiteite flake, the long axis of the leiteite crystal corresponded to the *b* axis, and the *a* axis was at right angles to the long axis. The Raman spectra of the oriented single crystals are reported in accordance with the Porto notation: the propagation directions of the incident and scattered light and their polarisations are described in terms of the crystallographic axes *a*, *b* and *c*. The notation may, for example read CABC. Here the first C is the direction of the incident light, A is the direction of the polarisation of the electric vector of the incident light, B is the orientation of the analyser and the second C is the direction of the propagation of the scattered light.

Infrared spectroscopy

Infrared spectra were obtained using a Nicolet Nexus 870 FTIR spectrometer. Spectra over the range 4000 to 550 cm^{-1} were obtained using the KBr beam splitter by the co-addition of 64 scans with a resolution of 2 cm^{-1} and a mirror velocity of 0.6329 cms^{-1}. Far infrared spectra were collected using the same spectrometer equipped with a polyethylene beam splitter replacing the KBr beam splitter. Samples (2 mg) were ground and intimately mixed with CsI (200 mg), followed by pressing it into a tablet at a pressure of 10 tonnes. Spectra were collected in transmission mode in a range from 120 to 600 cm^{-1}.

Spectral manipulation

Spectral manipulation such as baseline correction/adjustment was performed using the GRAMS software package (Galactic Industries Corporation, NH, USA). Band component analysis was undertaken using the Jandel 'Peakfit' software package that enabled the type of fitting function to be selected and allows specific parameters to be fixed or varied accordingly. Band fitting was done using a Lorentzian-Gaussian cross-product function with the minimum number of component bands used for the

fitting process. The Gaussian-Lorentzian ratio was maintained at values greater than 0.7 and fitting was undertaken until reproducible results were obtained with squared correlations of R^2 greater than 0.995.

RESULTS AND DISCUSSION

Description of crystal structure

Leiteite is monoclinic with space group $P2_1/c$ (C_{2h}^5) and four formula units per unit cell (a = 4.542, b = 5.022, and c = 17.597 Å) [1]. The structure consists of open Zn tetrahedral layer flanked on either side by single arsenite chains (Fig. 1) [1]. The [ZnO_4] tetrahedral share corners (O3 and O4) to form a checkerboard pattern. Similarly the arsenite groups also share corners (O1 and O2) to form chains. There are two distinct arsenite groups in the trigonal pyramidal geometry which alternate along the chain. Each As atom is thus connected to O1, O2, and either O3 or O4. O1 and O2 connect two As atoms and are termed bridging, while O3 and O4 connect As to Zn and thus are termed non-bridging with respect to As. The layers, connected by long As-O bonds, are stacked in the direction of c-axis. Positional parameters indicate all atoms are on general C_1 sites [1]. The non-bridging and bridging As-O bond lengths are 1.73 – 1.76 and 1.80 – 1.82 Å respectively.

Results of X-ray diffraction

The natural leiteite flakes and its synthetic snow white powder were subjected to XRD powder diffraction (Fig. S1). Although no impurities are observed in either pattern, confirming the absence of reinerite in the synthetic sample, there are relative intensity differences in the natural leiteite owing to the preferred orientation in the natural sample corresponding to the perfect (001) cleavage.

Scanning Electron Microscopy

The SEM image of the natural leiteite is shown in (Fig. S2a). Synthetic leiteite images show dandelion-like spheres (Fig. S2b). On closer examination the spheres appear to be made of small flakes. A possible explanation for this occurrence is the fact that the flakes of the synthetic crystals had not had time to grow into the large flakes such as those that appear in the natural sample.

Raman spectroscopy

Factor Group Analysis

The unit cell of leiteite is the primitive unit cell and it contains four formula units. Thus a primitive unit cell contains 28 atoms. The number of allowable modes is 81 consisting of $21A_g$, $21B_g$, $20A_u$, and $19B_u$. The analysis is represented in Table 1. The form of the polarisability tensor for C_{2h} crystals dictates that A_g modes are observed in the aa, bb, cc, and ac orientations and B_g modes in the ab and bc orientations. Thus it should be possible to assign a symmetry species to many of the Raman active modes.

The Raman spectra of leiteite are shown in Figs. 2 to 8. Figs. 2 and 3 show the non-oriented Raman spectra of natural and synthetic leiteite respectively. Figs. 4 – 8 show Raman spectra of an orientated single crystal of natural leiteite. The spectral results are displayed in Table 2. The intensities of the observed bands vary according to orientation allowing them to be assigned to either A_g or B_g modes as summarised in Table 3. A_g bands are generally the most intense in the CAAC spectrum, followed by ACCA, CBBC, and ABBA whereas B_g bands are generally the most intense in the CBAC followed by ABCA. The CAAC and ACCA spectra are identical, as are those obtained in the CBBC and ABBA orientations. Both cross-polarised spectra are identical.

After closer examination it was decided that the BACB and BAAB should not be used to determine band assignments. They are unreliable since they contain both A_g and B_g bands with intermediate intensities, for example bands at 169 (A_g), 181 (B_g), 201 (B_g), 207 (A_g), 258 (B_g), 270 (A_g), 305 (B_g), 370 (A_g), 550 (Bg), 603 (A_g), 651 (B_g), 764 (B_g), and 807 cm^{-1} (A_g) are all present in the above spectra. This is probably an indication of scrambling of the incident radiation, due to the biaxial nature of leiteite. Monoclinic crystals have one of the main optical directions (X, Y, and Z) of the indicatrix coincide with the b axis. The biaxial indicatrix is a triaxial ellipsoid containing the optical directions X, Y, and Z which are proportional to the refractive indices α, β, and γ respectively, listed in the order of decreasing ray velocity. Every section passing through the centre of this ellipsoid is an ellipse, except for two circular sections. The two directions normal to the circular sections are the optic axes which lie in the XZ plane. No birefringence is shown when light moves along the optic axes because it encounters the circular sections which have a constant refractive index β and thus, from the point of view of the light travelling along the axis, the crystal will seem isotropic. The acute angle between the two optic axes is defined by 2V or the optic angle. Leiteite is biaxially positive, α =1.87, β=1.88, γ =1.98. Biaxial positive indicates that the axis that

bisects the optic angle is the Z axis. Monoclinic crystals always have one if its principal optical directions (X, Y or Z) coincide with the *b* axis. In the case of leiteite this optical direction is Y. The angles between the *c* axis to Z and *a* axis to X are 10° and 11° respectively. Light travelling along the *b* axis will not encounter circular sections and will therefore experience birefringence.

The infrared spectra of leiteite are provided in the supplementary information. Fig. S3 shows the mid IR spectrum of natural leiteite. The synthetic leiteite gave an identical spectrum but is not shown here due to the presence of interference patterns. Fig. S4 shows the far IR spectrum of synthetic leiteite and unfortunately also exhibits interference patterns but is more presentable than the natural leiteite spectrum in the same region. The far IR spectrum could not be band fitted due to the lack of signal. The infrared spectra showed bands at 794, 765, 641, 609, 558, 462, 377, 370 – 360, 264, 254, 216, and 205 cm^{-1}. Upon closer examination, it was found that most of the Raman bands have a closely-spaced Davydov partner in the infrared spectrum. Davydov doublets are a result of weak layer-layer coupling, and contain either A_g-B_u or B_g-A_u pairs. By determining the mode of the Raman band, the mode of its infrared partner can be deduced, as summarised in Table 4.

The presence of the polymeric chain of AsO_2 instead of an isolated vibrating unit limits the value of factor group analysis in assigning the various arsenite modes. The stretching vibrations of the non-equivalent As-O bonds can be expected to give rise to $6A_g$ and $6B_g$ modes it is still not possible to resolve these modes due to the similarity of As-O bond lengths in the chain. 2 distinct As atoms x 3 non-equivalent As-O bonds x 4 formula units in a unit cell = 24 bands, which will split into $6A_g$, $6B_g$, $6A_u$, and $6B_u$. The form of the polarisability tensor for C_{2h} crystals dictates that A_g modes are observed in the aa, bb, cc, and ac orientations and B_g modes in the ab and bc orientations. Szymanski has previously assigned bands around 280 and 570 cm^{-1} to As-O-As vibrations [7], while Tossell [19, 20] assigned these vibrations to the region 490 – 550 cm^{-1}. Loehr and Plane [21] assigned the region 750 – 790 cm^{-1} to those of As-O. Keeping in mind that each vibration has an A_g and B_g component, some tentative band assignments have been made based on the oriented single crystal Raman spectra of leiteite. Bands at 310 (B_g), 370 (A_g), 458 (A_g) and 550 cm^{-1} (B_g) have been assigned to the stretching vibrations of the bridging As-O-As units, whereas bands at 600 (A_g), 650 (B_g), 763 (B_g) and 805 cm^{-1} (A_g) correspond to the stretches of non-bridging As-O. The deformation of the bridging As-O-As units may be found at 255 (B_g) and 270 cm^{-1} (A_g).

The polymeric arsenite chain appears as pictured in Fig. 1. A symmetric stretch of the bridging bonds may be envisaged as the As-O bonds of one As atom expanding while the bonds belonging to the As atoms next to it are contracting, and alternating in a concertina-like motion throughout the chain. An antisymmetric stretch may appear as one bridging As-O bond expanding while the other belonging to the same As atom contracts. We think the former vibration gives rise to the bands at 458 and 310 cm^{-1} and the latter to bands at 550 and 370 cm^{-1}. An Ag mode is simply caused by all four formula units in the unit cell vibrating in-phase, whereas in the case of a B_g mode the formula units across a mirror plane do not vibrate in-phase with each other.

Stretches of the non-bridging O are thought to vibrate in- or out-of-phase with the bridging ones, either in-phase being symmetric (805 and 650 cm^{-1}) or out-of-phase being antisymmetric (763 and 600 cm^{-1}). The observation of the symmetric stretch occurring at a higher frequency than the antisymmetric was confirmed in the matrix isolation of gaseous $NaAsO_2$ study by Gingerich and Bencivenni [22] and Ogden and Williams [23]. Although in the solid form $NaAsO_2$ exhibits similar polymeric arsenite chains, in the gaseous form Na^+ coordinates via two equivalent O atoms to As^{3+}, which makes the O atoms non-bridging (since they do not bridge two As atoms).

CONCLUSIONS

The A_g and B_g modes of leiteite $ZnAs_2O_4$ were successfully separated using Raman microscopy and an oriented single crystal. The assignment of bands in the mid and far IR spectra into Au and Bu modes were aided by the presence of Davydov doublets, which arise due to weak interlayer coupling. Most of the Raman bands were found to have an IR partner; those that do not may simply have a weak partner that is masked by interference patterns in the far IR spectrum. Band assignments were made with respect to bridging and non-bridging As-O bonds.

Acknowledgements

The financial and infra-structure support of the Queensland University of Technology Inorganic Materials Research Program of the School of Physical and Chemical Sciences is gratefully acknowledged. The Australian Research Council (ARC) is thanked for funding.

REFERENCES

[1] S. Ghose, P. K. Sen Gupta, E. O. Schlemper, *Amer. Min.* **1987,** *72,* 629-632.

[2] L. Bencivenni, K. A. Gingerich, *J. Mol. Struc.* **1983,** *99,* 23-29.

[3] B. Breidenstein, *Neues Jahr.Min., Monat.***1994,** 174-178.

[4] M. A. Cooper, F. C. Hawthorne, *Can. Min.* **1996,** *34,* 623-630.

[5] N. Y. Gubeladze, *Soobshcheniya Akademii Nauk Gruzinskoi SSR* **1982,** *108,* 337-340.

[6] O. Medenbach, W. Gebert, K. Abraham, *Neues Jahr.Min., Monat.* **1983,** 445-450.

[7] H. A. Szymanski, L. Marabella, J. Hoke, J. Harter, *Appl. Spectrosc.* **1968,** *22,* 297-304.

[8] F. Pertlik, *Tschermaks Min. Petr. Mitt.* **1975,** *22,* 211-217.

[9] F. Pertlik, *Tschermaks Min. Petr. Mitt.* **1977,** *436,* 201-206.

[10] R. Fischer, F. Pertlik, *Tschermaks Min. Petr. Mitt.* **1975,** *22,* 236-241.

[11] J. A. Krenner, *Zeit.Kristall.* **1921,** *56,* 198-200.

[12] M. Mellini, M. Amouric, A. Baronnet, G. Mercuriot, *Am. Min.* **1981,** *66,* 1073-1079.

[13] J. Sejkora, D. Ozdin, J. Vitalos, P. Tucek, J. Cejka, R. Duda, *Euro. J. Min.* **2007,** *19,* 419-427.

[14] S. Bahfenne, R. L. Frost, *Appl. Spectrosc. Rev.* **2010,** *45,* 101-129.

[15] S. Bahfenne, R. L. Frost, *J. Raman Spectrosc.* **2010,** *41,* 329-333.

[16] S. Bahfenne, R. L. Frost, *J. Raman Spectrosc.* **2010,** *41,* 465-468.

[17] R. L. Frost, S. Bahfenne, *J. Raman Spectrosc.* **2010,** *41,* 207-211.

[18] R. L. Frost, S. Bahfenne, *J. Raman Spectrosc.* **2010,** *41,* 325-328.

[19] J. A. Tossell, *Geochim. Cosmochim. Act.* **1997,** *61,* 1613-1623.

[20] J. A. Tossell, M. D. Zimmermann, *Geochim. Cosmochim. Act* **2008,** *72,* 5232-5242.

[21] T. M. Loehr, R. A. Plane, *Inorg. Chem.***1968,** *7,* 1708-1714.

[22] L. Bencivenni, K. A. Gingerich, *J. Mol. Struc.* **1983,** *99,* 23-29.

[23] J. S. Odgen, S. J. Williams, *J. Mol. Struc.* **1982,** *80,* 105-108.

List of Figures

List of Tables

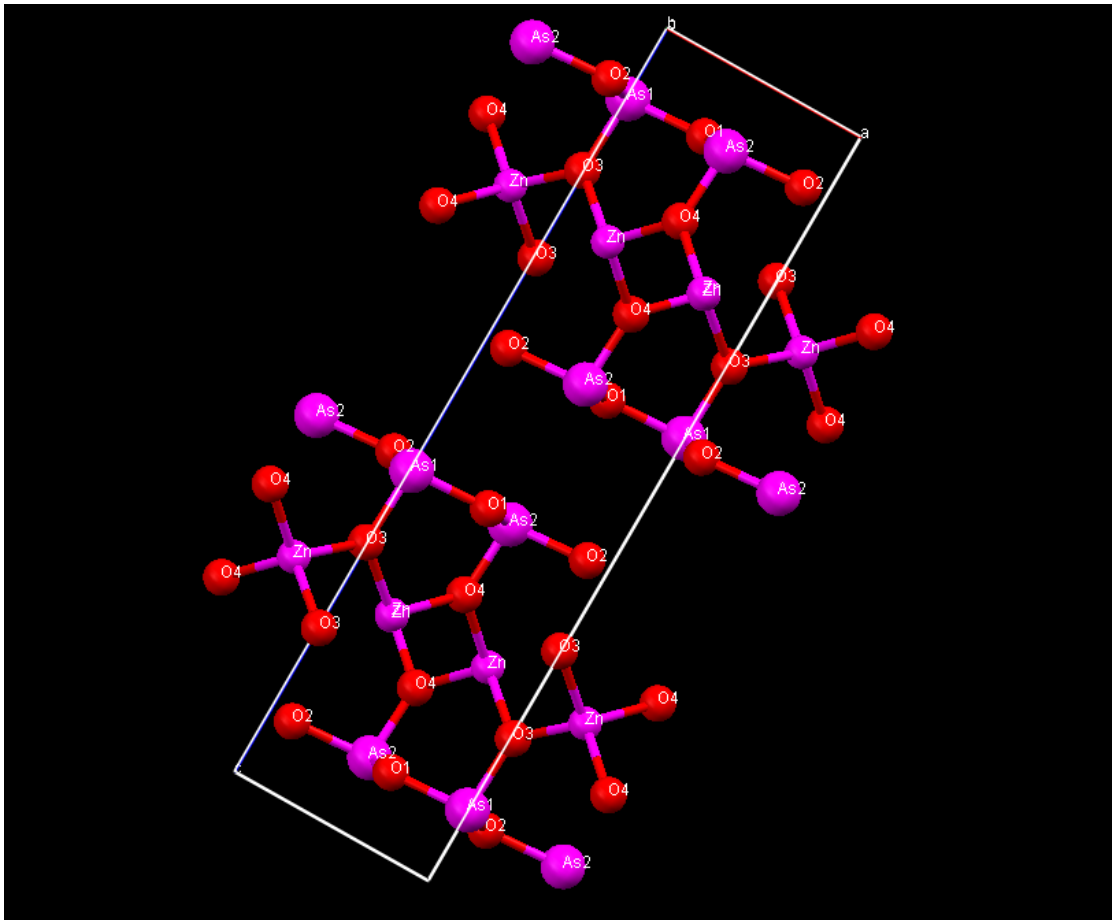

Fig. 1

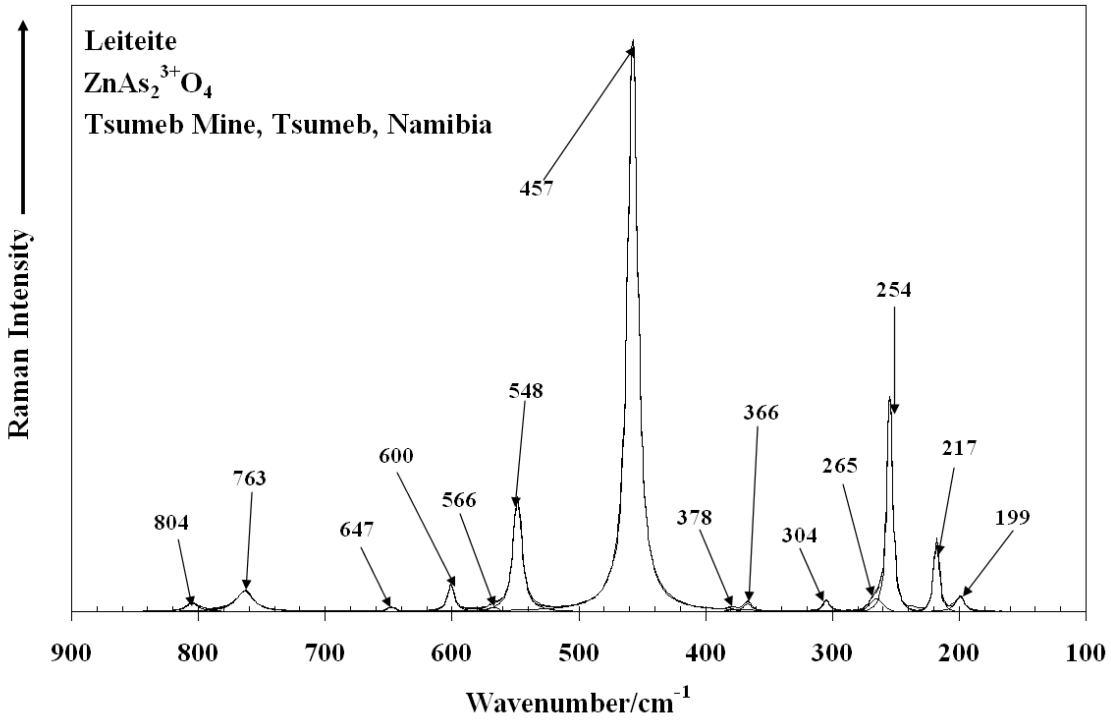
Leiteite
ZnAs2 3+O4
Tsumeb Mine, Tsumeb, Namibia
Raman Intensity
457
254
548
366
600
217
265
763
566
804
647
378
304
199
900
800
700
600
500
400
300
200
100
Wavenumber/cm-1

Fig. 2

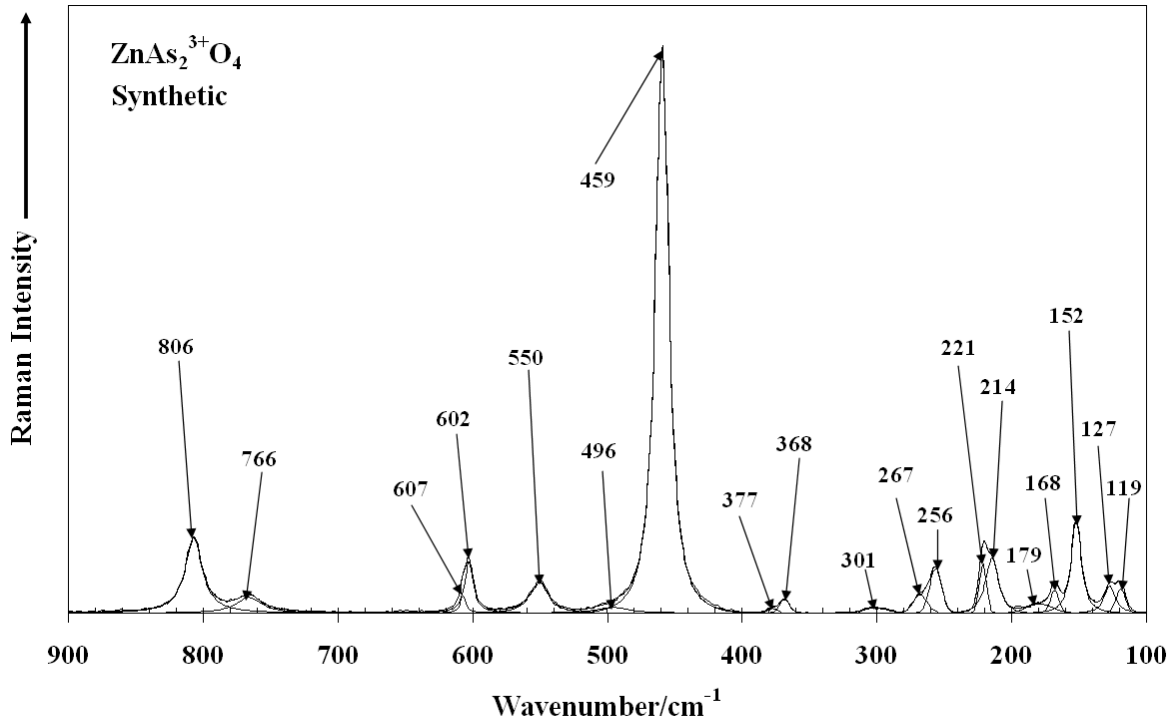
ZnAs2 3+O4
Synthetic
Raman Intensity
459
806
766
607
602
550
496
377
368
301
267
256
221
214
179
168
152
127
119
900
800
700
600
500
400
300
200
100
Wavenumber/cm-1

Fig. 3

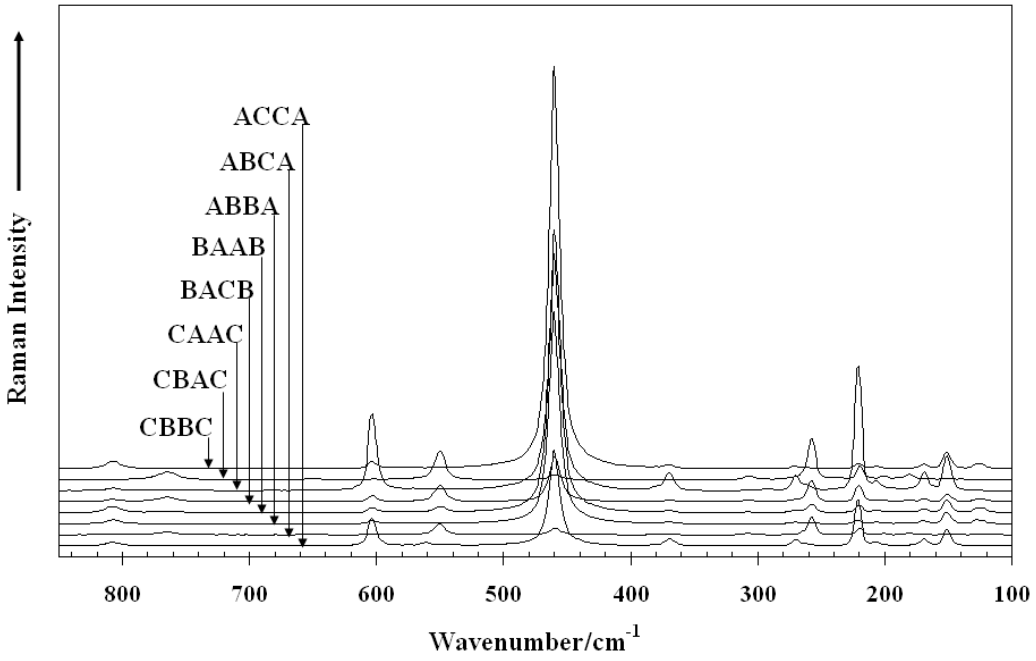
ACCA
ABCA
ABBA
BAAB
BACB
CAAC
CBAC
CBBC
Raman Intensity
800
700
600
500
400
300
200
100
Wavenumber/cm-1

Fig. 4

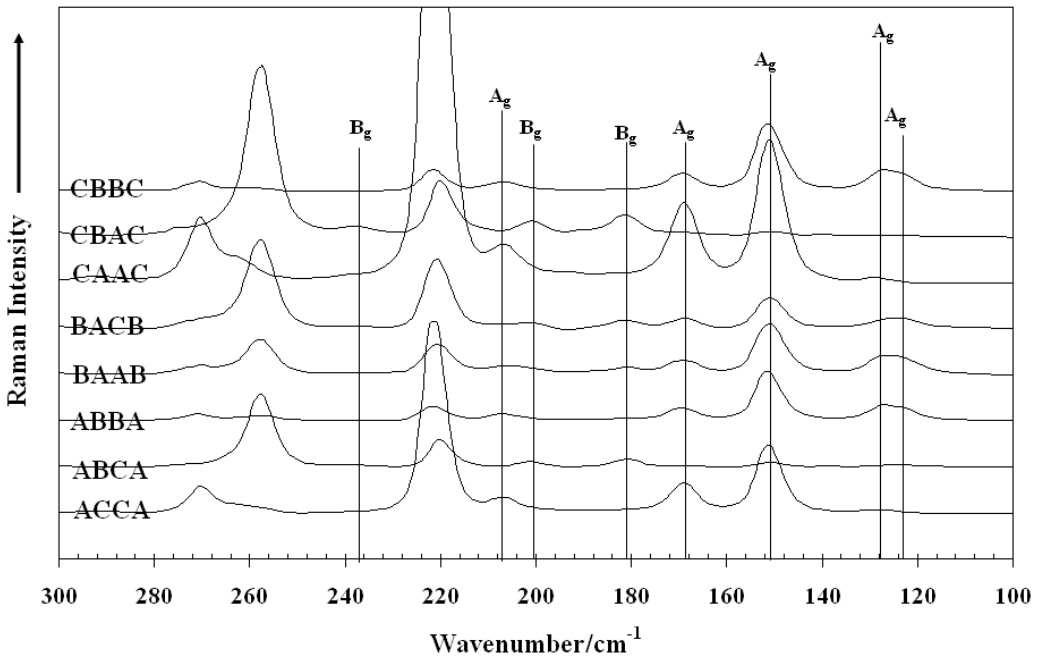
Raman Intensity
CBBC
CBAC
CAAC
BACB
BAAB
ABBA
ABCA
ACCA
B_g
A_g
B_g
B_g
A_g
A_g
A_g
300
280
260
240
220
200
180
160
140
120
100
Wavenumber/cm^{-1}

Fig. 5

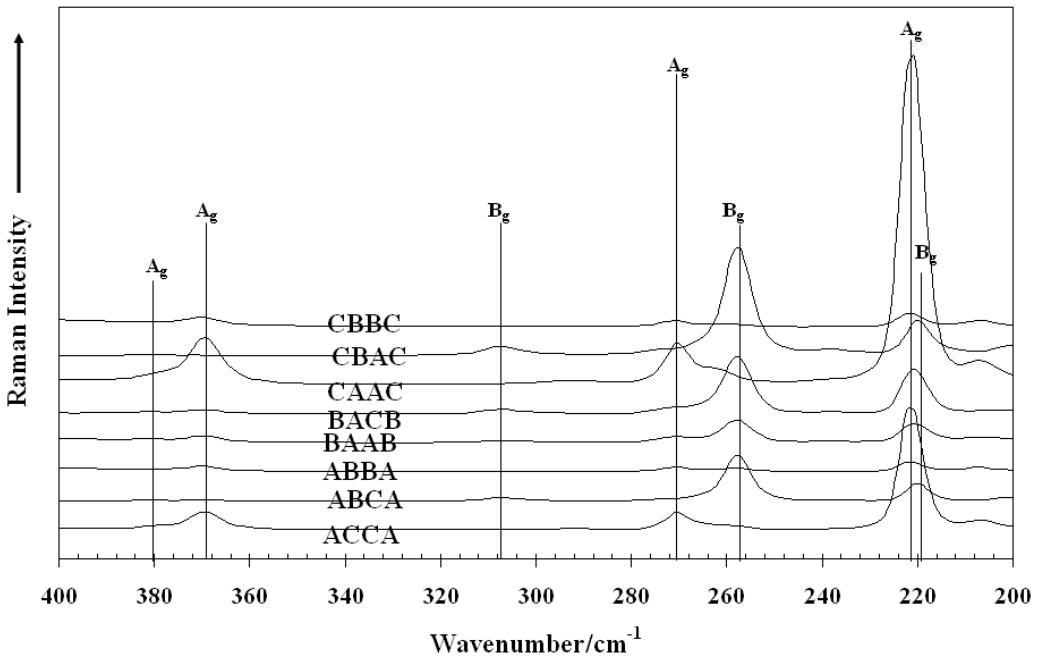
Raman Intensity
A_g
A_g
B_g
A_g
B_g
A_g
B_g
CBBC
CBAC
CAAC
BACB
BAAB
ABBA
ABCA
ACCA
400
380
360
340
320
300
280
260
240
220
200
Wavenumber/cm^{-1}

Fig. 6

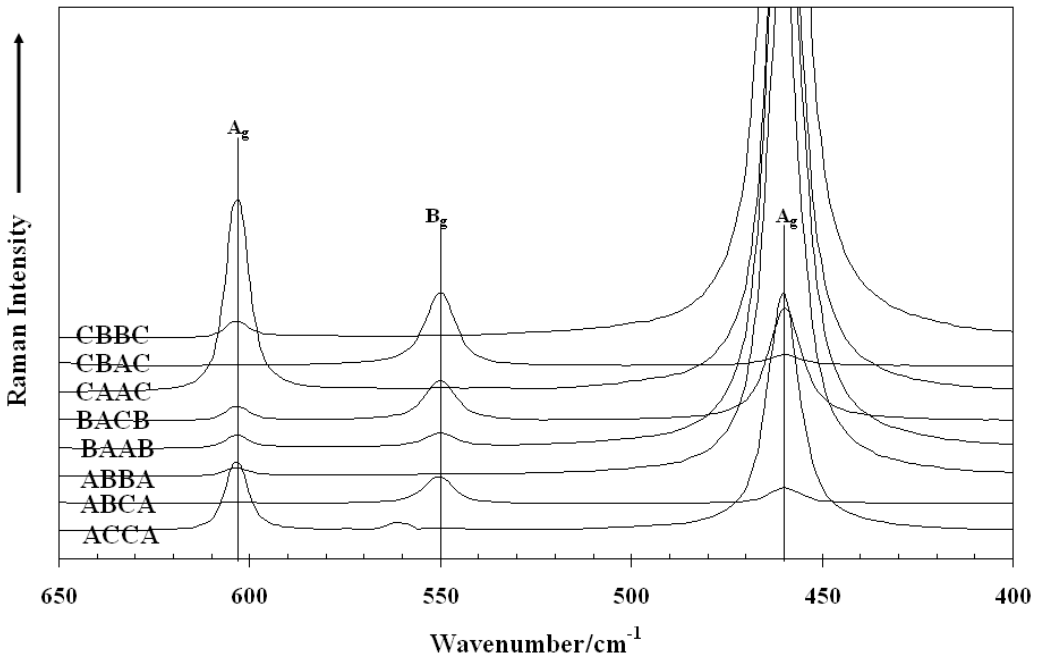
Raman Intensity
A_g
B_g
A_g
CBBC
CBAC
CAAC
BACB
BAAB
ABBA
ABCA
ACCA
650
600
550
500
450
400
Wavenumber/cm^{-1}

Fig. 7

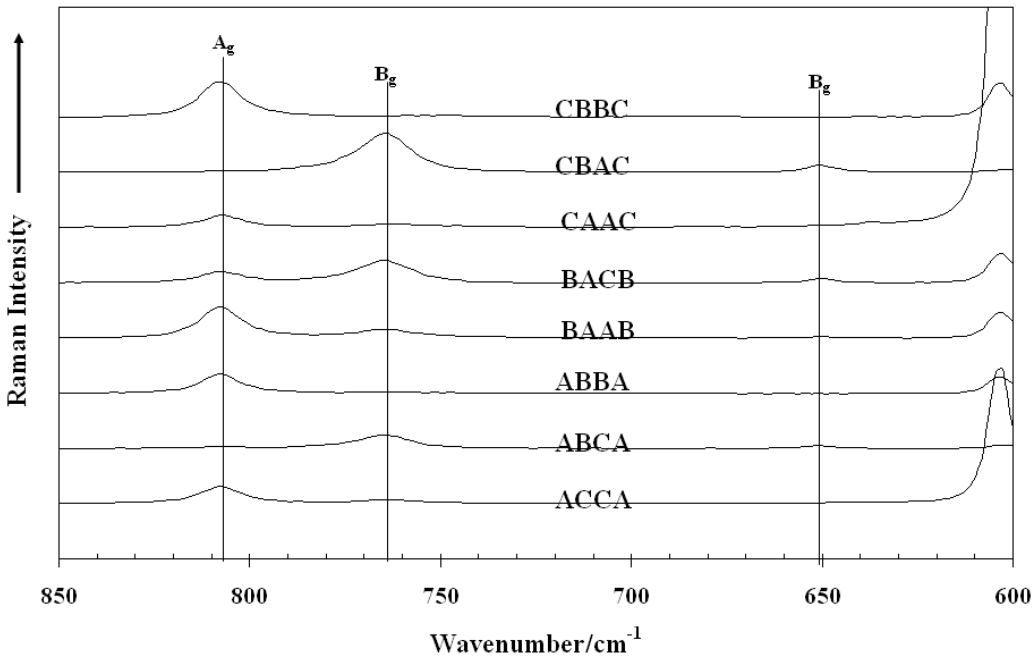
Ag
Bg
Bg
CBBC
CBAC
CAAC
BACB
BAAB
ABBA
ABCA
ACCA
Raman Intensity
850
800
750
700
650
600
Wavenumber/cm-1

Fig. 8

C_1 site symmetry	C_{2h} crystal symmetry	Translation
21A (7 atoms x 3A on each atom)	$21A_g$	
	$21B_g$	
	$21A_u$	T_z
	$21B_u$	T_{xy}

Table 1

CBBC			CBAC			CAAC			BACB			BAAB			ABBA			ABCA			ACCA		
Center	FWHM	%	Center	FWHM	%	Center	FWHM	%	Center	FWHM	%	Center	FWHM	%	Center	FWHM	%	Center	FWHM	%	Center	FWHM	%
																		109	5.02	0.12			
																		115	4.45	0.03			
123	6.19	0.12							121	3.96	0.18	122	6.35	0.46	122	5.29	0.36						
127	7.89	0.82	126	13.09	0.57	129	5.03	0.06	125	12.00	2.57	127	8.62	1.08	127	8.03	1.16	125	10.20	0.42	128	7.25	0.20
			139	5.71	0.15													139	5.45	0.24			
151	6.83	1.91	151	7.83	1.05	148	6.72	1.38	151	6.85	3.45	151	7.07	2.07	151	6.38	2.48	151	6.50	1.34	149	6.43	1.11
						151	5.70	2.69													152	5.01	2.64
169	6.92	0.72	168	7.42	0.54	169	6.87	2.76	169	6.95	1.17	169	7.46	0.81	169	7.51	1.01	169	6.76	0.46	169	6.77	2.99
			181	7.61	4.39				181	7.79	1.02	182	8.52	0.36				181	6.72	2.53			
			189	4.84	0.19																		
			201	8.72	3.38				201	5.72	0.44							201	5.22	1.96			
207	8.51	0.45				206	6.08	0.74	207	6.15	0.39	206	14.69	0.97	207	10.87	0.73				206	7.52	1.40
						216	43.80	2.65	218	6.81	2.97							218	9.02	2.45	219	5.59	5.10
221	5.95	0.50	220	5.90	7.54	219	5.08	4.19	221	5.59	5.05	220	6.65	1.04	221	6.04	0.64	220	4.76	4.83	222	4.70	8.12
						222	4.90	8.82															
			239	12.13	2.19				240	12.01	0.45	238	9.97	0.14				238	8.19	0.88			
																		249	14.61	1.08			
258	5.53	0.05	258	6.74	24.30				258	7.00	10.34	258	7.05	1.45	258	7.61	0.42	258	6.31	21.94			
263	6.14	0.05				262	7.63	0.83										266	12.55	3.24	261	9.92	0.71
271	5.75	0.33	270	16.27	3.27	270	6.17	1.58	269	11.38	1.70	270	8.47	0.57	271	6.46	0.44	307	8.44	2.09	270	5.86	1.67
						292	12.18	0.26	290	4.92	0.06										292	7.08	0.18
			305	10.73	1.97				304	14.54	0.57							307	8.44	2.09			
			308	6.35	1.56				308	7.04	0.50	306	6.15	0.13									
371	12.80	0.81	370	9.21	0.17	369	7.84	2.18	369	6.46	0.86	370	8.73	0.57	371	8.88	0.60	369	7.14	0.43	369	7.92	2.42
435	35.44	1.60	382	7.70	0.25	379	20.71	1.23	381	15.60	0.71							381	6.04	0.33	380	9.55	0.53
460	9.48	89.20	460	10.13	4.98	460	9.66	55.80	460	10.24	41.28	460	10.08	82.36	460	9.59	88.91	460	10.04	17.13	460	9.72	56.05
			507	94.47	0.89	499	18.39	0.46															
			550	8.62	17.60	542	42.66	1.08	550	9.58	13.04	550	11.70	2.18	550	12.55	0.28	550	8.28	15.72	561	6.08	0.60
			553	29.00	8.51	574	21.83	0.62															
			594	31.73	1.54	602	13.09	5.27															
603	7.69	1.26				603	6.21	5.74	603	7.10	4.00	603	7.19	1.26	603	6.97	0.81	603	7.77	1.19	603	8.52	6.72
																					604	6.00	4.02
			651	9.04	1.51				651	8.04	0.59							651	8.48	1.29			
			764	13.74	6.70	761	31.22	0.46	765	17.41	5.68	764	18.84	0.98	760	23.09	0.16	765	16.63	10.12	764	19.53	0.68
			769	32.77	7.51																		
808	12.54	2.17				807	12.68	0.69	807	14.68	2.96	808	12.33	2.52	808	11.96	2.00	807	19.61	1.69	808	13.04	2.68

Table 2

Band Centres/cm^{-1}	Suggested Assignment
123	Ag
127	Ag
139	Bg
151	Ag
169	Ag
181	Bg
201	Ag
207	Ag
220	Ag
239	Bg
258	Bg
270	Ag
305	Bg
370	Ag
381	Ag
460	Ag
550	Bg
603	Ag
651	Bg
764	Bg
807	Ag

Table 3

Raman	Assignment	IR	Assignment
201	Ag	205	Bu
207	Ag		
220	Ag	216	Bu
239	Bg		
258	Bg	254	Au
270	Ag	264	Bu
305	Bg	?	Au
370	Ag	360 - 370	Bu
381	Ag	377	Bu
460	Ag	462	Bu
550	Bg	558	Au
603	Ag	609	Bu
651	Bg	641	Au
764	Bg	765	Au
807	Ag	794	Bu

Table 4